

ANALYTICAL LOWER AND UPPER BOUNDS OF POWER ABSORPTION IN NEAR-FIELD REGIONS DEDUCED FROM A MODAL-BASED EQUIVALENT JUNCTION MODEL

B. Derat

SAGEM Communication (SAFRAN Group)
Mobile Phones R&D Department
2 rue du Petit Albi, 95801, Cergy-Pontoise, France

J.-Ch. Bolomey

SUPELEC
Electromagnetics Research Department
3 rue Joliot-Curie, 91192, Gif-sur-Yvette, France

Abstract—Due to the proximity of mobile phones to users' heads and resulting interrogations on potential health effects, as well as to the development of promising medical applications of electromagnetic waves such as non-invasive RF Hyperthermia treatments, near-field interactions between antennas and lossy scatterers, such as human beings, have been a topic of growing interest over the last decade. More generally, for various kinds of radiating sources and targets, much scientific effort has been done to answer the following question in particular configurations: what is the minimal/maximal power that can be absorbed in a lossy object located in the reactive field region of an antenna? The aim of this paper is to propose a general and analytical solution to this problem, applicable to any source-scatterer system. To this purpose, a method, allowing to describe power deposition mechanisms in near-field regions, is introduced. This approach is based on an equivalent junction/circuit model which is shown here to result from an appropriate modal expansion of the radiated field. The dual interpretation of this model in terms of localized circuit and lumped junction is used to demonstrate how trends and bounds in power absorption phenomena can be derived. Firstly, the analogy with the microwave circuit theory provides the concepts of available power and load factor for electromagnetic fields, which allow to highlight the parameters influencing power dissipation and to analyze consequent trends. Secondly, the junction matrix

formalism is used to obtain analytical lower and upper bounds of the power absorbed in a lossy object, located in the near field region of any radiating source. Those bounds give a clearer insight of the relationship between the total radiated power due to the antenna and the minimal or maximal power potentially dissipated in any scatterer exposed to such a radiated field. An example of bounds in a simple source-load configuration is finally provided, showing the link, to be further investigated, between the near-zone electric-field pattern of the antenna and the total dissipated power. This example also suggests that the power dissipated in a given object can be rapidly increased or reduced as the modal complexity of the source increases.

1. INTRODUCTION

Until now, numerical modeling has been almost exclusively used in order to predict the power dissipation resulting from near-field interactions between a source and a lossy object or scatterer [1–4]. However, the numerical approach does not provide more than the final calculated result for understanding power deposition mechanisms. Assessing the impact of various parameters may require an enormous quantity of calculation, without clear extrapolation possibility. However, beside this powerful but 'blind' approach, the development of simple models (e.g., [5–9]) has brought a significant support for a better understanding of loss mechanisms and related effects. Nevertheless, if those models provide some meaningful trends of power absorption phenomena, they only apply to particular sources, and are based on several approximations. Moreover, such techniques cannot be used to deduce general bounds of the minimal or maximal power absorbed in a lossy object, except in very specific configurations.

Bounds in electromagnetism have been a topic of growing interest for many years. In particular, many authors have pointed out the limitations of antennas in terms of bandwidth, directivity and efficiency [10–15]. Such limitations have shown to be really useful for designers, by highlighting the critical points to deal with and to what extent one can decrease their impact. Those very general limits have been essentially derived from appropriate modal field expansions. The objective of this paper is first to justify a general and analytical method for characterizing power transfer mechanisms, based on this modal field theory. According to this approach, the dissipation in any lossy scatterer can be described with an equivalent junction/circuit model, in terms of power transfer between a set of generators and a linear junction (multipole load). In order to point out common points

and differences between the classical microwave circuit theory and the proposed approach, the first section briefly reviews some important aspects of the power transfer between electrical generators and loads.

This section also provides some remarks concerning highly reactive generators, which are rarely mentioned in circuit books, yet useful to understand electromagnetic power dissipation in reactive near field regions. The next part demonstrates how the junction/circuit formalism can be transposed to electromagnetism by means of the modal field expansion. The concepts of available power and load factor for radiating sources and scatterers are introduced and discussed. As already shown in [16–19], those concepts are relevant to derive trends and bounds in power absorption mechanisms, when the problem can be modeled with a set of decoupled circuits. The interest of these quantities is here briefly highlighted and illustrated for simple source-scatterer configurations. However, for more complicated configurations, it may be necessary to use the junction formalism, which is shown here to provide a general formula for calculating the total dissipated power, as well as non-trivial lower and upper bounds of this power, for any lossy scatterer, in the presence of a given radiating source. Those bounds give a new point of view on the influence of the parameters limiting near-field energy deposition. Moreover, a simple example of these limits is given for a 2-D source-scatterer configuration, showing an interesting relationship between the total dissipated power and the shape of the near-zone electric field pattern. Finally, numerical calculation of the bounds for a specific load show that the lower (respectively upper) limit decreases (respectively increases) very rapidly with the modal complexity of the source.

2. POWER TRANSFER IN MICROWAVE CIRCUITS

2.1. Power Transfer between a Generator and a Load

All the complex voltages, currents and fields appearing in the text are peak values. Let E_g and $Z_g = R_g + jX_g$ be the ElectroMotive Force (EMF) and the internal impedance of a given generator. A complex load $Z_L = R_L + jX_L$ is connected to the generator; V and I are respectively the voltage across- and the current passing through- this load (Figure 1a). As well known, the active power P_d delivered to- or dissipated in- the load can be written as:

$$P_d = P_a \cdot \gamma_L \quad (1)$$

where P_a is the available power and γ_L is the load factor defined as follows:

$$P_a = |E_g|^2 / (8R_g) \quad (2)$$

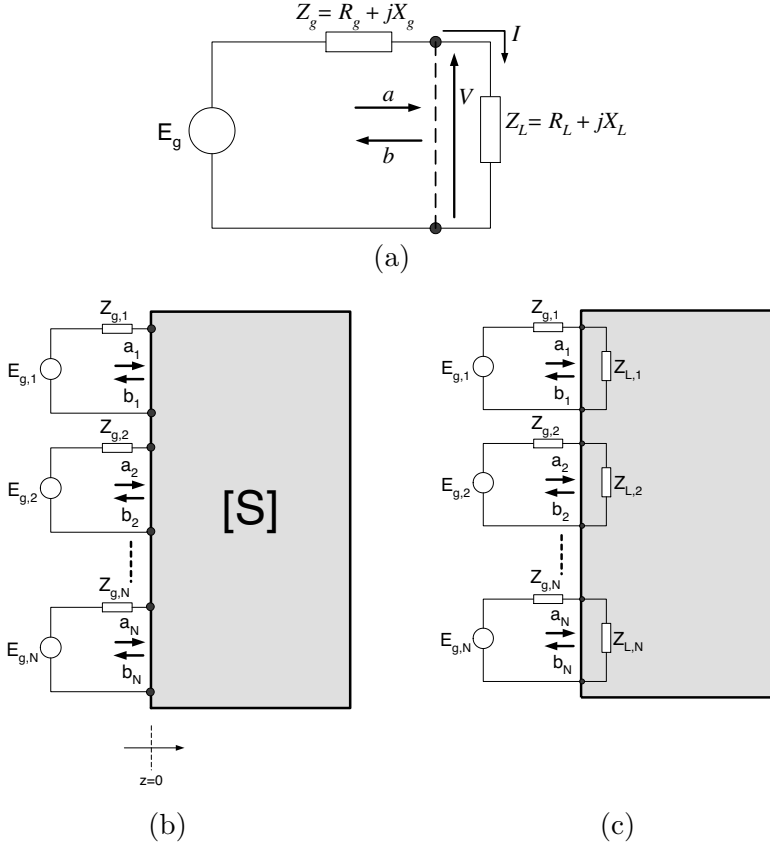


Figure 1. (a) Power transfer between a generator and a load. (b) Power transfer from a set of equivalent generators to a junction of scattering matrix $[S]$. (c) Power transfer from a set of equivalent generators to a junction of diagonal scattering matrix $[S]$, defining the equivalent circuit model.

$$\gamma_L = 1 - \left| \frac{(Z_L - Z_g^*)}{(Z_L + Z_g)} \right|^2 \quad (3)$$

The available power is the maximum active power that the generator can deliver to a load connected to its ports. Note that, as shown by (2), the available power only depends on the generator. The load factor is such that $0 \leq \gamma_L \leq 1$ and represents the efficiency of the power transfer from the generator to the load. The maximum power dissipation is obtained when the load factor is equal to 1, that is to say, when the impedance matching condition $Z_L = Z_g^*$ is satisfied.

The difference between the available power P_a and the actual dissipated power P_d may be considered as a “reflected” power P_r which is absorbed by the generator:

$$P_r = P_a - P_d \quad (4)$$

The standard voltage reflection coefficient ρ of the load is such that:

$$\rho = b/a = (Z_L - Z_g)/(Z_L + Z_g) \quad (5)$$

where a and b respectively represent the complex amplitudes of the incident and reflected voltage waves (Figure 1a). When Z_g is real, γ_L is simply related to ρ :

$$\gamma_L = 1 - |\rho|^2 \quad (6)$$

However, it is worth noting that when Z_g is complex (case of a reactive generator), the expression of the load factor is more complicated (see Appendix A):

$$\gamma_L = \left\{ 1 - |\rho|^2 - 2\chi \text{Im}(\rho) \right\} / \left\{ 1 + \chi^2 \right\} \quad (7)$$

where $\chi = X_g/R_g$. If $\chi = 0$, (7) reduces to (6). On the contrary, if the generator becomes purely reactive so that $|\chi| \rightarrow +\infty$ ($R_g \rightarrow 0$, E_g and X_g being assumed constant and non null), then the load factor goes to zero, whatever the load impedance (supposing the load is lossy). In any case, the load factor compensates the increase of P_a , which is proportional to χ and thus becomes infinitely large [19]. In that way, the power dissipated in the load remains always finite even if the available power tends to infinity. Note that, when the generator becomes purely reactive, it is more exact to say that the available power becomes “indefinite”, since the maximal power that can be transferred to the load only depends on the resistance of the load itself. As it will be noted in the following, these remarks are of crucial importance in the case of electromagnetic power transfer.

2.2. Power Transfer between a Set of Generators and a Multipole Load/Junction

The single circuit approach presented in Section 2.1 can be naturally extended to the case of a set of N generators directly connected to a linear junction J or multipole load (Figure 1b), uniquely determined by its normalized scattering matrix $[S]$. Such a matrix relates the complex amplitudes of the power normalized incident waves a_n to the power normalized reflected waves b_n , at each of the $n = 1, 2, \dots, N$ guiding structures, in the $z = 0$ reference plane of the junction

terminals (Figure 1b, the z -axis is oriented toward the junction and the $\exp(+j\omega t)$ convention is chosen), as follows:

$$(b) = [S](a) \quad (8)$$

Note that it is equivalent to consider that the incident waves of amplitudes a_n are due to N generators of EMF $E_{g,n} = 2\sqrt{R_n}a_n$ and impedances $Z_{g,n} = R_n + jX_n$ directly connected to J , or to N generators delivering incident waves of amplitudes $a'_n = a_n \exp(+jk_n Z)$ at the $z = Z$ reference plane, connected to J through transmission lines of propagation constants k_n and impedances $Z_{g,n}$. The n -th reflected wave amplitude b'_n at the $z = Z$ reference plane is then such as $b'_n = b_n \exp(-jk_n Z)$. Hence we consider here, without loss of generality, that the generators are directly connected to J . In such a case, the voltage V_n and current I_n at the n -th port of the load, can be related, as well known, to a_n and b_n as follows:

$$V_n = \sqrt{R_n} \cdot [a_n + b_n] \quad (9)$$

$$I_n = \sqrt{R_n} \cdot [a_n - b_n]/Z_{g,n} \quad (10)$$

By using equations (9) and (10), the total power P_d dissipated in J can be expressed such as:

$$P_d = \text{Re} \left(\frac{1}{2} \cdot \sum_{n=1}^N V_n I_n^* \right) = \sum_{n=1}^N P_{a,n} \cdot \gamma_{L,n} \quad (11)$$

where $P_{a,n} = |E_{g,n}|^2/(8R_n) = \frac{1}{2}|a_n|^2$ and $\gamma_{L,n} = \{1 - |\rho_n|^2 - 2\chi_n \text{Im}(\rho_n)\}/\{1 + \chi_n^2\}$ are the available power and load factor of the n -th circuit, with $\rho_n = b_n/a_n$ and $\chi_n = X_n/R_n$. If $[S]$ is diagonal, then $S_{mn} = \rho_n \delta_{mn}$ (S_{mn} is the coefficient of line m and column n of $[S]$; δ_{mn} is the Kronecker symbol) and ρ_n is the reflection coefficient at the n -th port of J . The problem in this case reduces to that of N independent generators delivering power to N distinct loads of impedance $Z_{L,n}$ (Figure 1c). $Z_{L,n}$ and ρ_n are related by means of (5).

3. APPLICATION OF THE MODAL EXPANSION TO THE CHARACTERIZATION OF POWER ABSORPTION IN NEAR FIELD REGIONS

3.1. Equivalent Junction Model Deduced from Modal Expansion

Power transfer from a radiating source to a lossy scatterer or load can be similarly described in terms of impedances, voltages and currents

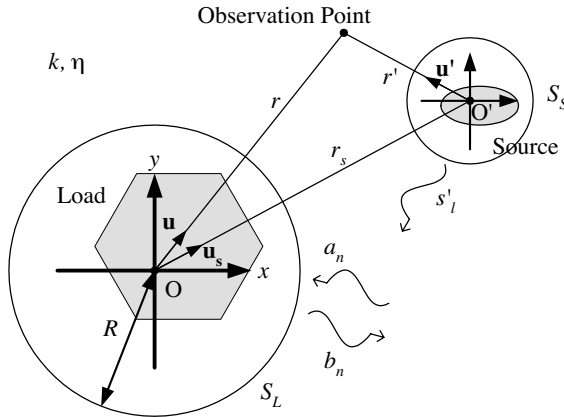


Figure 2. Source radiating in the presence of a lossy load, both surrounded by an homogeneous medium (wavenumber k and impedance η).

at the load terminals. The definition of those quantities and terminals is provided by the field modal expansion. Indeed, for any source contained in a cylindrical or spherical surface S_S centered on O' (Figure 2), the electric and magnetic fields on S_S can be expanded in a sum of elementary wave functions called “modes” [10, 13, 20, 21]. In a referential centered on O' said “attached” to the source, this modal expansion for a source in free space would only involve outgoing modes [10, 13, 20, 21]. Thanks to the addition theorem for radial wave functions (see e.g., [20, 22]), such a modal expansion can also be performed in any other coordinate system centered on O , distinct of O' ($OO' = r_s$) (Figure 2), on any cylindrical or spherical surface S_L centered on O . In such a coordinate system, the field expansion would involve incoming and outgoing modes, whatever the content of S_L (nothing or any scatterer).

It is then possible to consider that the incoming modes at the S_L surface carry an incident power from which the energy can be extracted by the scatterer or load (if any) in the $r < R$ region (Figure 2). The outgoing modes hence carry the power that has not been absorbed in the $r < R$ region and which can be viewed as “reflected”. As it is shown in the following, the incident power can be considered as provided, mode by mode, by an equivalent generator connected to a multipole load or microwave junction modeling the scatterer. Such a junction is fully characterized by its scattering matrix $[S]$, so that the scheme of Figure 1b can also be applied to the problem

of electromagnetic power transfer. Moreover, it is possible to define the concepts of modal available power and load factor for radiating sources and scatterers, by considering those quantities at each port of the equivalent junction, similarly to the circuit case (see Section 2.2). The total power dissipated in the scatterer is then obtained in the same way as (11). Note that if S_L is empty (free space) or contains a lossless scatterer, the total reflected power equals the total available power.

3.2. Power Transfer from an Electromagnetic Source to a Lossy Scatterer

Without loss of generality, the case of a Transverse Magnetic (TM) field to z in a cylindrical coordinate system centered on O or Transverse Electric field (TE) to r in a spherical coordinate system is now considered. In any coordinate system, the Transverse Electric (TE) field case is dual to the TM case and would be similarly treated.

It is assumed that the S_s and S_L surfaces (Figure 2) do not intersect each other and are surrounded by an homogeneous medium of wavenumber k and wave impedance η . In such a medium, the components \mathbf{E}_{tg} and \mathbf{H}_{tg} of the electromagnetic field, tangential to an appropriate coordinate surface of radius r centered on O , can be written as a combination of incoming and outgoing waves (the field is here assumed to be independent of z in the cylindrical problem) [20, 21]:

$$\mathbf{E}_{tg}(r, \mathbf{u}) = \frac{k}{\sqrt{K}} \cdot \sum_n \{ \alpha'_n F_n(kr) + \beta'_n G_n(kr) \} f_n(\mathbf{u}) \mathbf{e}_n(\mathbf{u}) \quad (12)$$

$$\mathbf{H}_{tg}(r, \mathbf{u}) = \frac{-k}{j\eta\sqrt{K}} \cdot \sum_n \{ \alpha'_n F'_n(kr) + \beta'_n G'_n(kr) \} f_n(\mathbf{u}) [\mathbf{u} \times \mathbf{e}_n(\mathbf{u})] \quad (13)$$

where \mathbf{u} denotes the unit radial vector pointing in the angular direction of the observation point (Figure 2). K is a normalization factor such that: $K = k^2 R p$ in the cylindrical case (p is the length of the cylinder portion considered), or $K = k^2 R^2$ in the spherical case. F_n and G_n are the radial harmonic functions of order n (dimensionless). $F'_n = d[F_n(kr)]/d(kr)$ in cylindrical coordinates and $F'_n = 1/(kr) \times d[kr F_n(kr)]/d(kr)$ in spherical coordinates [21]. Similarly, $G'_n = d[G_n(kr)]/d(kr)$ in cylindrical coordinates and $G'_n = 1/(kr) \times d[kr G_n(kr)]/d(kr)$ in spherical coordinates. F_n and G_n are chosen to respectively represent the incoming and outgoing waves in the selected coordinate system. $f_n(\mathbf{u})$ and $\mathbf{e}_n(\mathbf{u})$ respectively stand for the angular eigenfunction and the eigenvector of order n . F_n , G_n , f_n

and \mathbf{e}_n are known quantities in a given coordinate system [20]. The coefficients α'_n and β'_n are the complex amplitudes of the incoming and reflected waves, observed at the surface of radius r , for the n -th order mode. Those complex amplitudes are very similar to the a'_n and b'_n coefficients defined in Section 2.2. F_n and G_n account for propagation and play the same role as $\exp(\pm jk_n Z)$ in the circuit case. Moreover, in the same way as in the microwave network theory, it is possible to change the reference surface of observation, so that the tangential components of the field taken at the $r = R$ surface S_L , and given by (12) and (13), appear as expansions with respect to the angular harmonics $f_n(\mathbf{u})$:

$$\mathbf{E}_{tg}(r, \mathbf{u}) = \frac{k}{\sqrt{K}} \sum_n \{\alpha_n + \beta_n\} f_n(\mathbf{u}) \mathbf{e}_n(\mathbf{u}) \quad (14)$$

$$\mathbf{H}_{tg}(r, \mathbf{u}) = \frac{-k}{\sqrt{K}} \sum_n \{\alpha_n/Z_n^+ - \beta_n/Z_n^-\} f_n(\mathbf{u}) [\mathbf{u} \times \mathbf{e}_n(\mathbf{u})] \quad (15)$$

where $\alpha_n = \alpha'_n F_n(kR)$ and $\beta_n = \beta'_n G_n(kR)$ are respectively the amplitudes of the n -th order incoming and outgoing waves evaluated at the S_L surface. $Z_n^+ = j\eta F_n(kR)/F'_n(kR)$ and $Z_n^- = -j\eta G_n(kR)/G'_n(kR)$ are the corresponding wave impedances. It is then possible to respectively associate a voltage V_n and a current I_n to the electric and magnetic modal field components tangential to S_L , such that:

$$V_n = \alpha_n + \beta_n \quad (16)$$

$$I_n = \alpha_n/Z_n^+ - \beta_n/Z_n^- \quad (17)$$

Note that the knowledge of V_n and I_n for every mode order is sufficient to determine the field distribution in the whole space exterior to S_s and S_L . In the case where the medium surrounding the source and scatterer is lossless (k real), Z_n^+ and Z_n^- are shown to be conjugate [20]. This allows to write (16) and (17) in a form similar to (9) and (10) obtained in 2.2:

$$V_n = \sqrt{R_n} \cdot [a_n + b_n] \quad (18)$$

$$I_n = \sqrt{R_n} \cdot [a_n/Z_n^+ - b_n/Z_n^-] \quad (19)$$

where $|a_n|^2$ and $|b_n|^2$ have the dimension of power, and R_n is the real part of $Z_n^+ = R_n + jX_n$ and $Z_n^- = R_n - jX_n$. It is noteworthy that, even if the medium is lossless, the wave impedances are complex, so that Z_n^+ and Z_n^- are generally different. Those impedances are only equal at infinity and tend to the plane-wave impedance η of the medium.

This is due to the fact that the cylindrical or spherical wavefronts tend to be plane for large radii. Note that, for the sake of simplicity, the surrounding medium will now be considered as being lossless. However, the main rationales that follow are still valid in the case of a lossy medium.

First of all, note that the angular functions $f_n(\mathbf{u})$ are orthogonal over the $r = R$ surface, so that each mode is independent of the other ones at the exterior of S_L . In other words, it is possible to consider that the modal excitations are provided by N decoupled generators, where N is the number of modes considered to generate a non-negligible dissipated power (this number N will be discussed later in 3.4). It is then possible to model the lossy object by an equivalent N -ports electromagnetic junction J (multipole load), completely characterized by its normalized $N \times N$ scattering matrix $[S]$ defined at the S_L reference surface. This matrix verifies (8), with (a) and (b) being respectively the vectors containing the a_n and b_n modal coefficients for $1 \leq n \leq N$. Hence, the problem of electromagnetic power transfer between a source and a lossy scatterer appears as equivalent to the problem of power transfer between a set of generators and a lumped junction/multipole load, as represented on Figure 1b. For a separable lossy cylindrical or spherical scatterer, there is no mode conversion, so that the scattering matrix is diagonal in the appropriate coordinate system. In such a case, the equivalent junction model reduces to a set of N independent generators delivering power to distinct loads of impedance $Z_{L,n}$, as represented on Figure 1c.

Despite the strong link existing between the circuit and electromagnetic problems, it is worth noting that, the equivalent circuit/junction model verifies equations (18) and (19), which are generally different from (9) and (10), since Z_n^+ and Z_n^- are not generally equal, except when R tends to infinity. This difference impacts on many formulas resulting from (18) and (19). For instance, the expressions of the power dissipated in the junction J , the load factor, or the reflection coefficient are modified with respect to the classical circuit case (see Appendix A).

First, in the considered case of a lossless surrounding medium, the application of the Poynting theorem [20] and integration over the whole S_L surface, gives the following formula for the total power P_d dissipated in the load (see Appendix B):

$$P_d = \frac{1}{2} \operatorname{Re} \left(\sum_{n=1}^N V_n I_n^* \right) = \sum_{n=1}^N \frac{1}{2} |a_n|^2 \cdot \{1 - |\rho_n|^2\} / \{1 + \chi_n^2\} \quad (20)$$

where $\chi_n = X_n/R_n$, $\rho_n = b_n/a_n$. $f_n(\mathbf{u})\mathbf{e}_n(\mathbf{u})$ is supposed to be normalized in such a way that $\int_{\Omega} |f_n(\mathbf{u})|^2 \|\mathbf{e}_n(\mathbf{u})\|^2 d\Omega(\mathbf{u}) = 1$, where

$d\Omega$ is the elementary solid angle and Ω the total solid angle subtended by S_L . Similarly to the microwave network theory, the definition of the modal load factor $\gamma_{L,n}$ and power $P_{a,n}$ available at the S_L surface can be derived from (20):

$$P_{a,n} = \frac{1}{2}|a_n|^2 \quad (21)$$

$$\gamma_{L,n} = \left\{1 - |\rho_n|^2\right\} / \left\{1 + \chi_n^2\right\} \quad (22)$$

The dissipated power $P_{d,n}$ per mode of order n is then obtained as the product of $\gamma_{L,n}$ and $P_{a,n}$. The total power dissipated in the scatterer is the sum of all the $P_{d,n}$ over the N ports of J . The available power at each port of the junction can be viewed as provided by an equivalent generator of EMF $E_{g,n} = 2\sqrt{R_n}a_n$ and internal impedance $Z_{g,n} = Z_n^+$ (Z_n^- could be chosen as well; the following results would present slight differences, but the main ideas would be the same). It is noteworthy that the EMF and internal impedance of the equivalent generators (and hence the modal available power) are independent of the load if the surface S_L is fixed.

When the load is separable ($[S]$ is diagonal), the equivalent circuit model of Figure 1c applies. In such a case, ρ_n represents the reflection coefficient at the n -th port of the junction and can be related with the n -th order equivalent load impedance $Z_{L,n}$, such as (see Appendix A):

$$Z_{L,n} = V_n/I_n = Z_n^+(1 + \rho_n) / (1 - \rho_n (Z_n^+/Z_n^-)) \quad (23)$$

$$\rho_n = (Z_n^-/Z_n^+) \cdot (Z_{L,n} - Z_n^+) / (Z_{L,n} + Z_n^-) \quad (24)$$

As explained before, (22), (23) and (24) are different from analog equations in the classical transmission line theory (see (5) and (7)).

3.3. Load Factor for Electromagnetic Fields

It has been shown in [16–18] that the available power and load factor could be used to identify parameters impacting on the total dissipated power in a given scatterer, as well as to characterize and understand their impact. More than this, when the load is separable, the equivalent circuit of Figure 1c, thanks to the load factor concept, allows to obtain properties of minima and maxima of power absorption that can be reached with various sources and scatterers. Indeed, if one considers a given scatterer, the minimization (respectively maximization) of P_d requires that the source mostly excites the terminals presenting the lowest (respectively highest) load factors. Note that, as shown in (22), $\gamma_{L,n}$ directly decreases with the modulus of the reflection coefficient

and the reactance-to-resistance ratio χ_n of the modal generator. This formula shows that, even if the impedance $Z_{L,n}$ at the n -th port of the scatterer is well matched with that of the corresponding generator, modes above a given order transmit a negligible amount of power due to the high values of χ_n [20], imposing a low load factor.

Such a behavior is very different to that of microwave circuits. This is illustrated on Figure 3a and Figure 3b representing the load factors given by (7) and (22). As shown on Figure 3a, the load factor in circuit theory equals 1 if the $Z_L = Z_g^*$ matching condition is satisfied, whatever the reactance-to-resistance ratio of the generator. In the equivalent junction model, $\gamma_{L,n} = 1$ only if $\rho_n = 0$ and if the generator impedance is purely resistive. The second condition is only verified when S_L becomes infinitely large.

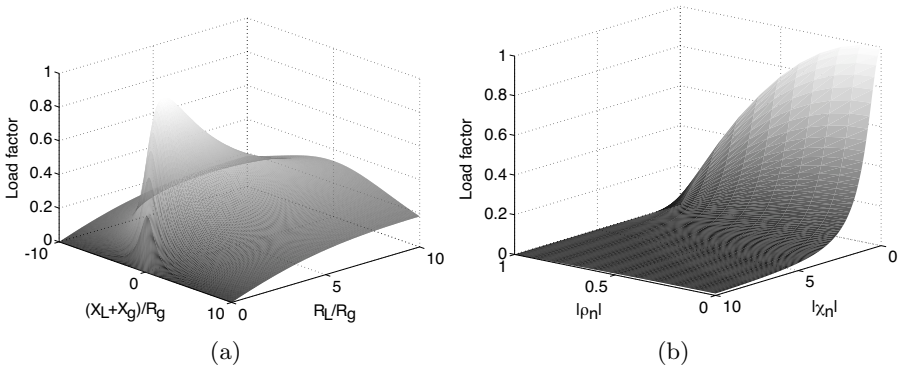


Figure 3. (a) Load factor given by (7) as a function of R_L/R_g and $(X_L + X_g)/R_g$. (b) Load factor given by (22) as a function $|\rho_n|$ and $|\chi_n|$.

For a given surface S_L containing a separable scatterer and a given frequency, $\gamma_{L,n}$ only depends on the geometrical and electrical characteristics of the lossy object. Modifying these parameters may significantly change the reflection coefficient ρ_n of a mode of given order n , but does not affect the χ_n parameter which only depends on k and S_L (the available power per mode is also unchanged). As an example, for a homogeneous scatterer whose conductivity σ varies from 0 to infinity, $\gamma_{L,n}$ will take all the values between 0 and a maximum value, which will necessarily be less than $1/(1 + \chi_n^2)$, and $P_{d,n}$ will follow these variations. In such a case, in order to minimize the power absorbed by the load, for instance, it is better to tune σ so as to increase the reflection coefficient of low order modes.

Figure 4a and Figure 4b illustrate the load factor and power transfer variations with conductivity. Figure 4a represents $\gamma_{L,0}$ as a function of conductivity, for an infinite cylindrical load of radius $R = 20$ mm and relative permittivity $\epsilon_r = 42.0$ (S_L is chosen to fit with the cylinder surface). Figure 4b shows P_d/P_{rad} variations also as a function of the conductivity of the same cylinder exposed to a uniform current line source at a distance of 10 mm ($r_s = 30$ mm). For both figures, the considered frequency is 900 MHz.

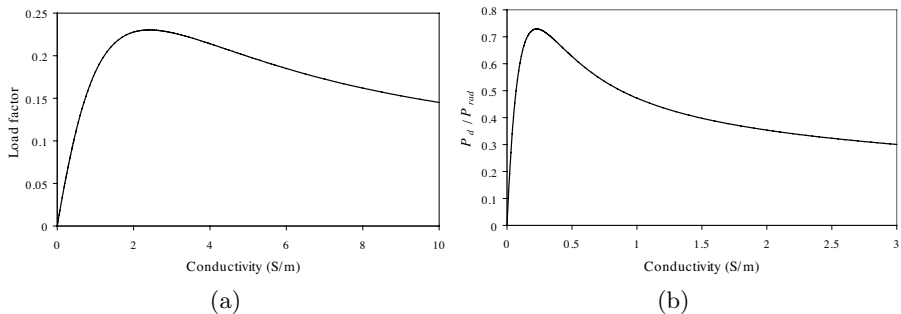


Figure 4. (a) Load factor of the zero order mode as a function of the conductivity of the cylindrical scatterer. (b) Ratio of the total dissipated power in the cylinder to total radiated power of the line source as a function of the load conductivity.

As observed, the load factor effectively passes through a maximum, as well as the power absorbed by the cylinder. These maxima do not generally coincide, except when the considered cylinder is sufficiently small to consider that only the zero order mode dissipates a significant power. In such a case, whatever the complexity of the source, power transfer in the near-field can be described with a single circuit. This particular configuration will be considered in more details in Section 4.2

3.4. Available Power for Electromagnetic Fields

The example of a cylindrical TM source exciting only the l -th order mode out of the S_s surface (Figure 2), in the coordinate system centered on O' , is now considered. S_s here denotes any cylinder centered on O' and containing the source. The couple (r_s, \mathbf{u}_s) indicates the position of the referential “attached to the source” in the referential centered on O . Without loss of generality, \mathbf{u}_s is assumed to be parallel to the x axis of this last coordinate system (Figure 2). By means of

(C3), the modal available power $P_{a,n}$ per unit length at the cylindrical surface of radius R can be simply expressed as follows (see (C5) of Appendix C):

$$P_{a,n} = \pi\eta k R P_{rad} \cdot \left| H_{n-l}^{(2)}(kr_s) \cdot H_n^{(1)}(kR) \right|^2 / (8R_n) \quad (25)$$

where P_{rad} is the power radiated per unit length by the source. Note that, for the sake of simplicity, the index n is now (and in the following) chosen symmetrical around 0. $H_{n-l}^{(2)}(kr_s)$ is the Hankel function of the second kind and order $n-l$, taken at kr_s ; $H_n^{(1)}(kR)$ the Hankel function of the first kind and order n , taken at kR . By means of (C9), one can show that:

$$P_{a,n} = \frac{1}{2} |a_n|^2 \geq \frac{1}{2} |a_n|^2 / (1 + \chi_n^2) = \frac{P_{rad}}{4} |H_{n-l}^{(2)}(kr_s)|^2 \quad (26)$$

Since the right member of (26) diverges as n goes to infinity, $P_{a,n}$ also goes to infinity. The fact that the available power diverges as the mode order increases can be related to the similar behavior in the circuit case (2.1). As a matter of fact, the higher is the mode order the more the equivalent generator becomes reactive. In the limit case of an infinitely reactive generator having no internal resistance but a non-zero EMF, the available power becomes infinite, and more exactly “indefinite”. Indeed, the available power is the active part of power that one could obtain at most, by connecting a load to the generator terminals. Such an upper bound value is not determined in the case of a purely reactive generator: the maximal power that can be transferred to the load only depends on the resistance of the load. To illustrate this behavior of the modal available power, Figure 5a represents $P_{a,n}/P_{rad}$ on the surface of a $R = 50$ mm 2-D cylinder, exposed to the field radiated by a uniform current line source (zero-order mode). The line source is located parallel to the cylinder axis and at 10 mm from its surface. The frequency of operation is 900 MHz. Those parameters will be used for the computation of other quantities in this section.

On the other hand, as explained in Section 3.3, the load filters high order modes presenting a high available power with a very low load factor. This is observed on Figure 5b representing the modal load factor for the same 2-D cylinder example, with $\varepsilon_r = 42.0$ and $\sigma = 1$.

A consequence is that only a finite number N of modes generates a non negligible dissipated power and the concept of available power for modes of order much greater than N has no clear interest. In the case of an homogeneous cylindrical or spherical load, N can be evaluated by using arguments similar to those developed by Harrington [20; p. 309], or Hansen in [21; p. 17]. Actually, due to the cut-off properties of Bessel

functions, the field modes of orders n such as $|n| > |k_L|R$ [16–18] (k_L is the wavenumber inside the load), must weakly contribute to the total dissipated power. As a consequence, in such a configuration, one can take N as $2N_{max} + 1$, where $N_{max} = \lceil |k_L|R \rceil$ denotes the first integer larger than $|k_L|R$. If a better accuracy is needed for the calculation of P_d , then N_{max} can be taken equal to $\lceil |k_L|R \rceil + n_1$. In general, a number n_1 smaller than 10 is sufficient [21].

Figure 5c illustrates that the modes of order higher than N_{max} only participate to a small amount of the total dissipated power. In the chosen case of cylinder-line source configuration, $N_{max} = 7$. As observed on Figure 5a, b, and c, for modes of order n such that $n > N_{max}$, the available power increases exponentially with n , whereas the load factor and dissipated power decrease exponentially.

4. LOWER AND UPPER BOUNDS OF DISSIPATED POWER IN A LOSSY SCATTERER

4.1. General Derivation of the Lower and Upper Bounds of Dissipated Power

The arguments of Harrington [20] and Hansen [21] were originally applied to characterize the modal distribution of the electromagnetic field exterior to a volume containing an antenna. Indeed, as shown in [21], if S_s is the minimal cylindrical or spherical surface of radius R' centered on O' (Figure 2) containing the source, then the modes of orders $|l| > L = \lceil kR' \rceil$, in the referential centered on O' , must be strongly attenuated outside S_s . Only $2L + 1$ modes are hence to be considered in order to describe the field exterior to S_s , in a sufficiently

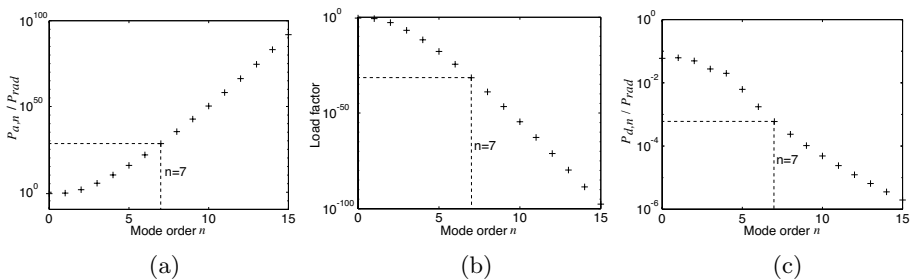


Figure 5. (a) Available power normalized to total radiated power as a function of the mode order. (b) Load factor as a function of the mode order. (c) Dissipated power normalized to total radiated power as a function of the mode order.

accurate way. If a better accuracy is needed, one can slightly increase the number of modes considered.

As a consequence, for $r' > R'$, the tangential components of the fields due to an antenna exciting TM cylindrical waves or TE spherical waves, can be expanded in the appropriate coordinate system, in a finite weighted sum of $2L+1$ outgoing wave functions, in the referential centered on O' :

$$\mathbf{E}_{\mathbf{t}g}(r', \mathbf{u}') = \frac{k\sqrt{\eta}}{\sqrt{K'}} \cdot \sum_{l=-L}^{+L} s'_l G_l(kr') f_l(\mathbf{u}') \mathbf{e}_l(\mathbf{u}') \quad (27)$$

$$\mathbf{H}_{\mathbf{t}g}(r', \mathbf{u}') = \frac{-k}{j\sqrt{\eta K'}} \cdot \sum_{l=-L}^{+L} s'_l G'_l(kr') f_l(\mathbf{u}') [\mathbf{u}' \times \mathbf{e}_l(\mathbf{u}')] \quad (28)$$

where s'_l is the spectral coefficient of the l -th source mode on the S_s surface, in the referential centered on O' . The “source vector” (s') of the s'_l coefficients is normalized, thanks to the K' factor, such that $P_{rad} = \frac{1}{2} \|(s')\|^2 = \frac{1}{2} \sum_{l=-L}^{+L} |s'_l|^2$. \mathbf{u}' denotes the unit radial vector pointing in the angular direction of the observation point (Figure 2).

As explained in 3.1, the power available at the S_L surface can be calculated by applying the addition theorem for radial wave functions [20, 22] (S_s and S_L are assumed to have no intersection). In a very general manner, the addition theorem can be expressed in matrix formulation as follows (it can be directly seen from (C3) or (C5), for example):

$$(a) = [A](s') \quad (29)$$

where $[A]$ is a matrix with an infinite number of lines and $2L+1$ columns. Here the $[A]$ matrix represents the transformation of TM waves in the cylindrical coordinate system centered on O' (respectively TE waves in spherical coordinates) into TM waves (respectively TE waves) in the O centered referential. Another matrix should be defined to characterize the TM (respectively TE) to TE wave (respectively TM) transformation. Note that, in a cylindrical coordinate system, it is possible to choose the referentials related with the source and load, so that the field may be TM or TE in both referentials. Then, only one matrix can be considered. In such a coordinate system, the coefficients A_{nl} of the $[A]$ matrix can be deduced from (C5). Due to what was explained in 3.4, when S_L contains a lossy scatterer, $[A]$ can be considered as a finite rectangular matrix of size $(2N_{\max}+1) \times (2L+1)$. For the sake of simplicity, the indices n and l of the vectors are chosen symmetrical around 0 ($|n| \leq N_{\max}$, $|l| \leq L$). It is noteworthy that $[A]$ only depends on the coordinate system, the kr_s product, the \mathbf{u}_s vector, and the load and source volumes (through kR and kR').

After (8), (20) and (29), the total power P_d dissipated in the junction can be written as a scalar product, such as:

$$P_d = \frac{1}{2} {}^t(s')^* {}^t[A]^* \{ [D] - {}^t[S]^*[D][S] \} [A](s') = \frac{1}{2} {}^t(s')^* [U](s') \quad (30)$$

where ${}^tX^*$ denotes the transposed conjugate of any X vector or matrix. $[D]$ is a diagonal matrix with coefficients $D_{nn} = 1/(1 + \chi_n^2)$. This formula is very general and allows to compute the total dissipated power due to any source in any scatterer, supposing that the modal coefficients of the source are known as well as the scattering matrix of the load. It can be observed that $[U] = {}^t[A]^* \{ [D] - {}^t[S]^*[D][S] \} [A]$ is a definite positive hermitian matrix of dimension $(2L + 1) \times (2L + 1)$. Indeed, it is possible to show that ${}^t[U]^* = [U]$ and that P_d in a lossy scatterer is always strictly positive except for trivial cases (no source excitation or infinitely small load). It is hence possible to apply the spectral theorem for hermitian matrices [23, 24] claiming that $[U]$ admits real eigenvalues $\xi_{-L}, \xi_{-L+1}, \dots, \xi_{+L}$ and that an orthonormal basis of associated eigenvectors $u_{-L}, u_{-L+1}, \dots, u_{+L}$ exists. Furthermore, since $[U]$ is definite positive, all the eigenvalues are strictly greater than 0. The source vector (s') can be expressed in the basis of the eigenvectors such as $(s') = \sum_{l=-L}^{+L} \zeta_l u_l$. By using this expression in (30), the following equation is obtained:

$$P_d = \frac{1}{2} \sum_{l=-L}^{+L} \xi_l |\zeta_l|^2 \quad (31)$$

If ξ_M (resp. ξ_m) is the maximum (resp. minimum) eigenvalue, then P_d verifies the following inequality:

$$\xi_m P_{rad} \leq P_d \leq \xi_M P_{rad} \quad (32)$$

These bounds of P_d give a new point of view on the parameters limiting the power absorbed by a lossy scatterer exposed to field radiated by an electromagnetic source. Actually, in a given coordinate system, ξ_m and ξ_M depend on the wavelength in the surrounding medium (through k), the distance between the antenna center of phase and scatterer (through r_s), the source and load volumes (through N_{\max} , L , and R), and the electrical parameters (through $[S]$) of the lossy object. Those eigenvalues do not depend on the source radiation characteristics (the (s') vector). As a consequence, assuming that the frequency of operation, the surrounding medium, the lossy scatterer and the distance between the source and load volumes are fixed, the previous inequalities show that the minimal and maximal power potentially

dissipated in the scatterer are only determined by the power radiated by the source P_{rad} and do not depend on the fine modal distribution of the source excitation (it is only related with the norm of the source vector). Moreover, these bounds show a separate dependence on the source and scatterer. Note that the detailed structure of the antenna only imposes how far is the power P_d effectively dissipated in the scatterer from the lower and upper limits. Those limits can be reached with particular sources whose (s') vectors are eigenvectors related to extreme eigenvalues.

4.2. Dissipated Power Bounds in a Simple 2-D Source-Scatterer Configuration

The meaning of the eigenvectors and eigenvalues obtained in the previous paragraph is not obvious. In order to have a better understanding of these quantities, it can be interesting to study a simple source-scatterer configuration, for which explicit values can be calculated. To this purpose, the case of a very small cylinder exposed to the field of a TM source is here considered.

First, the expression of P_d in such a configuration can be simply derived from (C10), by taking only the $n = 0$ contribution into account. By applying the Cauchy-Schwartz theorem [23], one can obtain a feasible upper bound of P_d :

$$P_d \leq \frac{P_{rad}}{4} \sum_{l=-L}^{+L} \left| H_l^{(2)}(kr_s) \right|^2 \cdot \{1 - |\rho_0|^2\} \quad (33)$$

This upper bound is coherent with the maximal eigenvalue ξ_M of the $[U]$ matrix, whose coefficients are given by (C12). This can be shown by solving the characteristic equation of $[U]$ [23]. Such a bound is reached for a source whose modal coefficients s'_l are such that:

$$s'_l = \frac{\left[H_{-l}^{(2)}(kr_s) \right]^*}{\sqrt{\sum_{l=-L}^{+L} \left| H_l^{(2)}(kr_s) \right|^2}} \sqrt{2P_{rad}} \quad (34)$$

By inserting this expression in (C1), one obtains the tangential component of the electric field due to this source at $r' = r_s$, in its attached coordinate system:

$$E_z(r_s, \theta') = \frac{k\sqrt{\eta P_{rad}}}{\sqrt{\pi K'}} \frac{1}{\sqrt{\sum_{l=-L}^{+L} \left| H_l^{(2)}(kr_s) \right|^2}}$$

$$\cdot \left\{ \left| H_0^{(2)}(kr_s) \right|^2 + 2 \sum_{l=1}^{+L} (-1)^l \left| H_l^{(2)}(kr_s) \right|^2 \cos(l\theta') \right\} \quad (35)$$

The very small cylinder is supposed to be located at $\theta' = \pi$, so that E_z in this direction can be simplified into:

$$E_z(r_s, \pi) = \frac{k\sqrt{\eta P_{rad}}}{\sqrt{\pi k R'}} \sqrt{\sum_{l=-L}^{+L} \left| H_l^{(2)}(kr_s) \right|^2} \quad (36)$$

Since the considered cylinder is small, the power absorbed by this load, for a portion of length p , exposed to the field of (36), can also be calculated as follows:

$$P_d = \pi R^2 p \times \frac{\sigma |E_z(r_s, \pi)|^2}{2} = \frac{-\pi R^2 \text{Im}(k_L^2) P_{rad}}{4} \sum_{l=-L}^{+L} \left| H_l^{(2)}(kr_s) \right|^2 \quad (37)$$

σ is the conductivity of the cylinder. This equation is coherent with the upper bound value of (33) and gives an approximation of $(1 - |\rho_0|^2)$ as R tends to zero.

Note that the upper bound of (33) can also be interpreted in E-field terms. Indeed, by directly applying the Cauchy-Swartz theorem to (C1), one can show that (36) also defines the maximal feasible electric field magnitude in a given direction, at $r' = r_s$. An antenna generating the maximal absorbed power in the small cylindrical load is hence an antenna which maximizes the electric field magnitude in the direction of the load. This behavior is illustrated on Figure 6a, representing the electric field magnitude near-zone pattern at $r' = r_s$, for L between 0 and 3, and $P_{rad} = 1$ W. For computing this figure, the radius of the cylinder is chosen to be $R = 0.1$ mm, r_s is set equal to 10 cm, and the frequency of operation is 900 MHz. The electrical characteristics of the cylinder are the same as those used in 3.3. $r_s = 10$ cm does not mean that the distance between the source and scatterer is 10cm, but that the maximal possible cylinder containing the source has a radius of $R' = r_s - R \approx 10$ cm. As explained in 4.1, this distance limits the maximal order of modes L to be taken into account to $kR' \approx 2$ or a little more (here $L = 3$ is considered at most).

Note that, as shown on Figure 6a, for $L = 0$, the source is omnidirectional and the power absorbed by the load is directly proportional to the radiated power P_{rad} (see (C11)). For L greater than zero, the peak of electric field magnitude is clearly observed in the direction of the load. On the other hand, as the cylinder tends to be infinitely small, the dissipated power tends to zero. However,

as long as the source has a non-zero volume the null dissipated power can never be reached, so that the lower bound of P_d should be strictly positive.

We have assumed here that we could consider only the zero order mode in the load referential. However this truncation results in an approximation of P_d . Because of this approximation, the lower bound of P_d can be shown to be equal to zero. However, this is not the case in real configurations where higher order modes (in the load referential) always contribute to the dissipated power. As a consequence, it is here possible to find non-trivial s'_l coefficients such that $P_d = 0$, but in fact they are such that P_d tends to 0. A set of such coefficients can be expressed as follows (see (C10)):

$$s'_l = \begin{cases} \sqrt{P_{rad}/L} & , \text{if } l > 0 \\ 0 & , \text{if } l = 0 \\ (-1)^{l+1} \sqrt{P_{rad}/L} & , \text{if } l < 0 \end{cases} \quad (38)$$

Inserting these coefficients in (C1) allows to obtain the following E-field expression:

$$E_z(r_s, \theta') = \frac{jk\sqrt{2\eta P_{rad}}}{\sqrt{\pi L K'}} \sum_{l=1}^{+L} |H_l^{(2)}(kr_s)|^2 \sin(l\theta') \quad (39)$$

The modulus of E_z as given by (39) is represented on Figure 6b as a function of θ' , for $L = 1$ to 3, and $P_{rad} = 1$ W. The same configuration as for the Figure 6a is used. On the opposite of the sources generating the maximal absorbed power, these sources are such that a minimum of E-field occurs at the load location.

So as to have order of magnitudes of the minimal and maximal eigenvalues ξ_m and ξ_M in the specific configuration studied here, these quantities have been calculated numerically either by using the first equality of (37), or by computing the ‘‘eigen-sources’’ defined by [U]. A very good agreement between these formulas have been noticed for the evaluation of ξ_M . However, only the matrix formulation allows to correctly assess ξ_m , since it takes into account modes of order greater than zero in the load referential. Figure 7a represents ξ_m and ξ_M eigenvalues as functions of the maximal source order L considered.

Logically, since the cylinder is very small, even the maximal power possible to dissipate with a source of order $L = 3$ is very weak. However, it is interesting to notice that the upper bound of dissipated power increases exponentially with L , and so decreases the lower bound. This means that, for reasonable source orders (relatively to the source volume), the power absorbed in a small cylinder can be

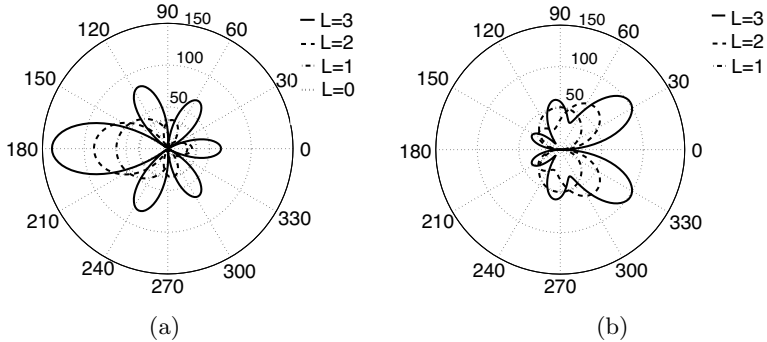


Figure 6. (a) $|E_z(r_s, \theta')|$ given by (35) as a function of θ' , for a maximal mode order $L = 0$ to 3. $P_{rad} = 1$ W. (b) $|E_z(r_s, \theta')|$ given by (39) as a function of θ' , for a maximal mode order $L = 1$ to 3. $P_{rad} = 1$ W.

increased or reduced exponentially, as the modal complexity of the source is increased.

The calculation of the eigenvalues and eigenvectors of the $[U]$ matrix has also been performed for a much larger cylinder ($R = 50$ mm), with a maximal source volume of radius 15 cm ($r_s = 20$ cm), and similar results have been found. Indeed, the “eigen-sources” minimizing or maximizing P_d exhibit quite similar near-zone patterns as those represented on Figure 6a and Figure 6b, as shown on Figure 7b. Particularly, antennas maximizing power absorption present a peak of E-field magnitude at $r' = r_s$, in the direction $\theta' = \pi$ of the center of the load. Antennas minimizing power absorption present a hole of E-field at this location. Moreover, ξ_m and ξ_M have been noticed to show the same exponential decrease / increase as represented on Figure 7a.

5. CONCLUSION AND PERSPECTIVES

This paper shows how the modal field expansion leads to an equivalent junction model, providing a new way to describe and quantify power transfer mechanisms between an antenna and a lossy object. The introduction of the concepts of available power and load factor for sources and scatterers gives a different point of view on the parameters impacting on power absorption. Under certain conditions, those concepts allow to separate the load and source influence on dissipation and to determine general trends in power loss phenomena. This technique also provides a general formula to calculate the dissipated power in a lossy object, as well as meaningful bounds on the possible

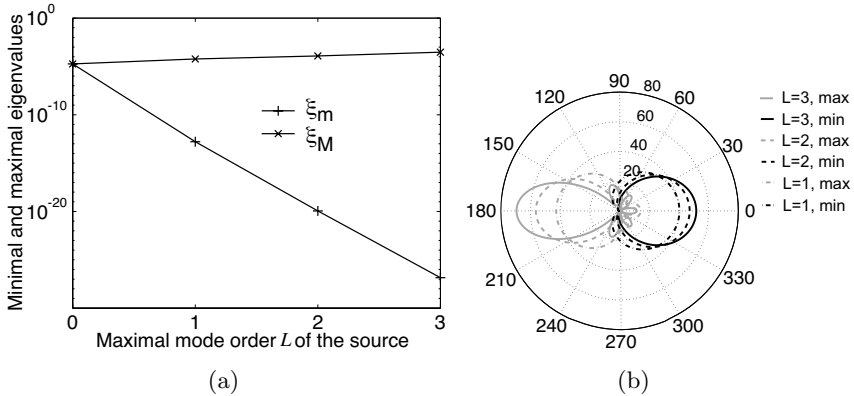


Figure 7. (a) Minimal ξ_m and maximal ξ_M eigenvalues for the small cylinder exposed to a TM source exciting modes of order $\pm L$, at most. (b) $|Ez(r_s, \theta')|$ as a function of θ' , for “eigen-sources” of maximal mode order $L = 1$ to 3 , giving the minimal ξ_m and maximal ξ_M eigenvalues. The load is a cylinder of radius $R = 50$ mm. $r_s = 20$ cm, $P_{rad} = 1$ W.

range of variation of dissipated power. The obtained limits are very general and do not suppose any particular characteristics of the source or load, except that the source behavior is not significantly affected by the load presence (interactions are neglected). The lower and upper bounds derived with this method are interesting in many ways. First, they are realizable with particular sources of calculable characteristics. Second, their expressions show that the antenna and scatterer have a separate influence on the minimal and maximal power potentially absorbed. Indeed, for a given frequency and volume containing the source, the only antenna parameter influencing those limits is the total radiated power, which multiplies a term depending only on the lossy scatterer and its distance to the source. Finally, the computation of these bounds in a simple configuration suggests that an interesting relationship exists between the electric field magnitude in the near-zone of an antenna and the total dissipated power. Indeed, it is observed in this configuration that antennas maximizing power absorption present a peak of electric-field in the direction of the load. The opposite is observed for antennas minimizing power absorption. Moreover, it is also noticed that, under given conditions, the minimal and maximal power potentially dissipated can be reduced/increased exponentially by increasing the modal complexity of the source. Future work will study the variations of those bounds with the source-scatterer configurations and try to give numerical results in other particular

cases. A special interest will be shown in extending these trends and bounds to the characterization of more realistic situations, such as human exposure in the near-field of mobile phones, base-station antennas, or non-invasive RF hyperthermia treatments, for instance. Among others, the equivalent junction model should give meaningful directions for tentatively solving the particular problem of averaged SAR minimization or maximization, which has become of more and more crucial importance (e.g., [25]).

APPENDIX A. DERIVATION OF EXPRESSIONS (7) AND (22) OF THE LOAD FACTOR FOR MICROWAVE CIRCUITS AND ELECTROMAGNETIC FIELDS

Suppose that Figure 1a can either represent a classical single circuit or an equivalent circuit modeling the power transfer of a given mode, as described in Section 3. First, in the circuit case, equations (9) and (10) applied to this simple system can be written as follows:

$$V = \sqrt{R_g} \cdot [a + b] \quad (\text{A1})$$

$$I = \sqrt{R_g} \cdot [a - b]/Z_g \quad (\text{A2})$$

By combining $P_d = \frac{1}{2}\text{Re}\{VI^*\}$ with (A1) and (A2), one obtains:

$$P_d = \frac{R_g}{2}\text{Re}\left\{\left(|a|^2 - |b|^2 + 2j\text{Im}(a^*b)\right)/Z_g^*\right\} \quad (\text{A3})$$

After a few manipulations, P_d can be written such as:

$$P_d = \frac{1}{2}|a|^2 \cdot \left\{\left(1 - |\rho|^2\right)\text{Re}\left(R_g/Z_g^*\right) + 2\text{Re}\left(j\text{Im}(\rho)R_g/Z_g^*\right)\right\} \quad (\text{A4})$$

where ρ is defined by (5). R_g/Z_g^* can be expressed as a function of the reactance-to-resistance ratio of the generator $\chi = X_g/R_g$ such that:

$$R_g/Z_g^* = \frac{1}{1 + \chi^2} + j\frac{\chi}{1 + \chi^2} \quad (\text{A5})$$

Inserting (A5) in (A4) allows to extract the expression of the load factor γ_L as given by (7).

In the electromagnetic case, equations linking V and I to a and b are different, as shown by (18) and (19). Applied to the single circuit case of Figure 1a, these formulas are such that:

$$V = \sqrt{R_g} \cdot [a + b] \quad (\text{A6})$$

$$I = \sqrt{R_g} \cdot [a/Z_g - b/Z_g^*] \quad (\text{A7})$$

By combining $P_d = \frac{1}{2}\text{Re}\{VI^*\}$ with (A6) and (A7), one obtains:

$$P_d = \frac{R_g}{2}\text{Re}\left\{\left|a\right|^2/Z_g^* - \left|b\right|^2/Z_g + 2j\text{Im}\left(a^*b/Z_g^*\right)\right\} \quad (\text{A8})$$

The term $\text{Re}(j\text{Im}(a^*b/Z_g^*))$ is null, so that (A8) gives:

$$P_d = \frac{1}{2}\left|a\right|^2 \cdot \left\{\text{Re}\left(R_g/Z_g^*\right) - \left|\rho\right|^2 \cdot \text{Re}\left(R_g/Z_g\right)\right\} \quad (\text{A9})$$

Inserting (A5) in (A9) allows to obtain the expression of the load factor as in (22). Formula (23) for the load impedance Z_L is simply obtained from (A6) and (A7), as the ratio of V over I . (24), giving the reflection coefficient ρ as a function of Z_L and Z_g , is directly obtained by equating V and $Z_L I$.

APPENDIX B. APPLICATION OF THE POYNTING THEOREM TO THE DETERMINATION OF (20)

Equation (1-62, p. 22) of [20] provides a formulation of the Poynting theorem applied to a source-free region. Taking The real part of this equation allows to show that the power P_d dissipated in the load contained in S_L (Figure 2) can be written such that:

$$P_d = -\frac{1}{2}\text{Re}\left(\int_{S_L} \mathbf{E}_{\mathbf{t}\mathbf{g}} \times \mathbf{H}_{\mathbf{t}\mathbf{g}}^* u dS\right) \quad (\text{B1})$$

By using expressions (14) and (15) for the electric and magnetic tangential components, as well as the orthogonality of wavemodes on the S_L surface, one obtains:

$$P_d = \frac{k^2}{2K}\text{Re}\left(\sum_n \{\alpha_n + \beta_n\} \{\alpha_n^*/Z_n^- - \beta_n^*/Z_n^+\} \cdot \int_{S_L} (f_n(\mathbf{u})\mathbf{e}_n(\mathbf{u})) \times (f_n^*(\mathbf{u})[\mathbf{u} \times \mathbf{e}_n^*(\mathbf{u})]) u dS\right) \quad (\text{B2})$$

After some manipulations on the vector products, the integral term can be simply expressed as follows:

$$\begin{aligned} \int_{S_L} (f_n(\mathbf{u})\mathbf{e}_n(\mathbf{u})) \times (f_n^*(\mathbf{u})[\mathbf{u} \times \mathbf{e}_n^*(\mathbf{u})]) u dS \\ = \frac{S_L}{\Omega} \int_{\Omega} |f_n(\mathbf{u})|^2 \|\mathbf{e}_n(\mathbf{u})\|^2 d\Omega(\mathbf{u}) \end{aligned} \quad (\text{B3})$$

where Ω is the total solid angle subtended by S_L and $d\Omega$ is the elementary solid angle. In spherical coordinates, S_L and Ω are simply related by $S_L = \Omega R^2$. In cylindrical coordinates, for a cylinder portion of length p , $S_L = \Omega p R$. With an appropriate normalization of the angular eigenfunctions and eigenvectors, namely $\int_{\Omega} |f_n(\mathbf{u})|^2 |\mathbf{e}_n(\mathbf{u})|^2 d\Omega(\mathbf{u}) = 1$, the integral term of (B2) can be set equal to S_L/Ω . In Section 3.2, K is defined such as $K = k^2 S_L/\Omega$. Hence, by using also (16) and (17), the following formulation for P_d is obtained:

$$P_d = \frac{1}{2} \text{Re} \left(\sum_n (\alpha_n + \beta_n) \{ \alpha_n^*/Z_n^- - \beta_n^*/Z_n^+ \} \right) = \frac{1}{2} \text{Re} \left(\sum_n V_n I_n^* \right) \quad (\text{B4})$$

(B4) is the same relationship as (20). By changing (16) and (17) into (18) and (19), and making similar manipulations as in Appendix A, the right member of (20) is directly obtained from (B4).

APPENDIX C. APPLICATION OF THE EQUIVALENT JUNCTION MODEL TO THE DETERMINATION OF THE TOTAL DISSIPATED POWER IN A 2-D SOURCE-SCATTERER CONFIGURATION

For the sake of simplicity, a cylindrical source exciting only TM modes is considered. It is also assumed that the referentials attached to the source and load (Figure 2) have parallel axes. The angle between \mathbf{u}_s and x (see Figure 2) is supposed to be null. In such a configuration, equations (27) and (28) can be written as follows [20; p. 200–202]:

$$E_z = \frac{k\sqrt{\eta}}{\sqrt{K'}} \sum_{l=-L}^{+L} s'_l H_l^{(2)}(kr') \frac{\exp(jl\theta')}{\sqrt{2\pi}} \quad (\text{C1})$$

$$H_{\theta'} = \frac{k}{j\sqrt{\eta K'}} \sum_{l=-L}^{+L} s'_l H'_l{}^{(2)}(kr') \frac{\exp(jl\theta')}{\sqrt{2\pi}} \quad (\text{C2})$$

where (r', θ') is the couple of cylindrical coordinates in the referential attached to the source. $H_l^{(2)}(kr')$ and $H'_l{}^{(2)}(kr')$ are respectively the Hankel function of second kind and order l , and its first derivative. K' is a normalization factor such as $K' = 2kp/\pi$, which allows to obtain $\frac{1}{2} |(s')|^2 = P_{rad}$ (p is the length of the considered cylinder portion). The addition theorem for Hankel functions of any order [22] is then applied to “translate” modes in the referential attached to the source,

into modes in the referential attached to the load (Figure 2). This addition theorem can be expressed as follows:

$$H_l^{(2)}(kr') \exp(jl\theta') = \sum_{n=-\infty}^{+\infty} H_{n-l}^{(2)}(kr_s) J_n(kr) \exp(jn\theta) \quad (C3)$$

$J_n(kr) = \frac{1}{2}\{H_n^1(kr) + H_n^2(kr)\}$ is the Bessel function of the first kind and order n , and $H_n^{(1)}(kr)$ the Hankel function of the first kind and order n . Utilizing (C3) in (C1) provides the following expression of E_z in the load referential:

$$E_z = \frac{k}{\sqrt{K}} \sum_{n=-\infty}^{+\infty} \frac{\sqrt{\eta K}}{2\sqrt{K'}} \left[\sum_{l=-L}^{+L} s'_l H_{n-l}^{(2)}(kr_s) \right] \cdot \left\{ H_n^{(1)}(kr) + H_n^{(2)}(kr) \right\} \frac{\exp(jn\theta)}{\sqrt{2\pi}} \quad (C4)$$

In the cylindrical case, K is such that $K = k^2 R p$. From equations (5–18, p.202) of [20] and (C4), H_θ can be directly obtained. Note that (C4) is similar to (12). Hence, applying this formula to the case where $r = R$ and using the definition of a_n resulting from (14), (16) and (18), one obtains:

$$a_n = \frac{1}{\sqrt{R_n}} \frac{\sqrt{\eta K}}{2\sqrt{K'}} \left[\sum_{l=-L}^{+L} s'_l H_{n-l}^{(2)}(kr_s) \right] \cdot H_n^{(1)}(kR) \quad (C5)$$

One can directly derive from (C5) the available power for the mode of order n , thanks to (21). On the other hand, by applying (A5) to Z_n^- , the incident power at the n -th port of the junction can be expressed by:

$$\frac{1}{2} |a_n|^2 / (1 + \chi_n^2) = \frac{\eta K}{8K'} \left| \sum_{l=-L}^{+L} s'_l H_{n-l}^{(2)}(kr_s) \right|^2 \cdot \left| H_n^{(1)}(kR) \right|^2 \operatorname{Re} \left(1/Z_n^- \right) \quad (C6)$$

The real part of $1/Z_n^-$ can also be written in terms of Hankel functions:

$$\operatorname{Re} (1/Z_n^-) = \frac{1}{\eta |H_n^{(1)}(kR)|^2} \operatorname{Re} \left(-j \left(H_n^{(1)}(kR) \right)^* H_n^{\prime(1)}(kR) \right) \quad (C7)$$

Using the Wronskian of Bessel's equation (D-17, p.463 of [20]), (C7) can be simplified such that:

$$\operatorname{Re} (1/Z_n^-) = 2 / \left[\pi \eta k R \left| H_n^{(1)}(kR) \right|^2 \right] \quad (C8)$$

Inserting (C8) in (C6) provides the following formulation of the incident power:

$$\frac{1}{2} |a_n|^2 / (1 + \chi_n^2) = \frac{1}{8} \left| \sum_{l=-L}^{+L} s'_l H_{n-l}^{(2)}(kr_s) \right|^2 \quad (\text{C9})$$

Supposing that the modes generating a significant dissipation are such that $|n| \leq N_{\max}$, and using (C9) in (20) allows to obtain the following expression for the power dissipated in the load:

$$P_d = \sum_{n=-N_{\max}}^{+N_{\max}} \frac{1}{8} \left| \sum_{l=-L}^{+L} s'_l H_{n-l}^{(2)}(kr_s) \right|^2 \cdot \left\{ 1 - |\rho_n|^2 \right\} \quad (\text{C10})$$

In case of a source exciting only the mode of order l , (C10) can be simplified in the following way:

$$P_d = \frac{P_{rad}}{4} \sum_{n=-N_{\max}}^{+N_{\max}} \left| H_{n-l}^{(2)}(kr_s) \right|^2 \cdot \left\{ 1 - |\rho_n|^2 \right\} \quad (\text{C11})$$

Finally note that (C10) allows to obtain analytical expressions for the coefficients U_{ij} of the $[U]$ matrix (see (30)) in the case of a separable load:

$$U_{ij} = \frac{1}{4} \sum_{n=-N_{\max}}^{+N_{\max}} H_{n-i}^{(1)}(kr_s) H_{n-j}^{(2)}(kr_s) \cdot \left\{ 1 - |\rho_n|^2 \right\} \quad (\text{C12})$$

ACKNOWLEDGMENT

The authors wish to thank R. Alliot and C. Leray at SAGEM Communication for having provided industrial means to explore such theoretical issues, as well as for their general support.

REFERENCES

1. Jensen, M. A. and Y. Rahmat Samii, "EM interactions of handset antennas and a human in personal communications," *Proc. IEEE*, Vol. 83, 7–17, 1995.
2. Manteuffel, D., A. Bahr, P. Waldow, and I. Wolff, "Numerical analysis of absorption mechanisms for mobile phones with integrated multiband antennas," *Proc. of IEEE Antennas Propag. Symp.*, 82–85, 2001.

3. Rowley, J. T. and R. B. Waterhouse, "Performance of shorted microstrip patch antennas for mobile communication handsets at 1800 MHz," *IEEE Trans. Antennas Propag.*, Vol. 47, No. 5, 815–822, 1999.
4. Onishi, T., T. Iyama, and S. Uebayashi, "The estimation of the maximum SAR with respect to various types of wireless device usage," *Proc. of EMC Zurich*, 151–154, 2005.
5. Kuster, N. and Q. Balzano, "Energy absorption mechanism by biological bodies in the near field of dipole antennas above 300 MHz," *IEEE Trans. on Vehicular Tech.*, Vol. 41, No. 1, 17–23, 1992.
6. Vainikainen, P., J. Ollikainen, O. Kivekäs, and I. Kelder, "Resonator-based analysis of the combination of mobile handset antenna and chassis," *IEEE Trans. Antennas Propag.*, Vol. 50, No. 10, 1433–1444, 2002.
7. Kivekäs, O., J. Ollikainen, T. Lehtiniemi, and P. Vainikainen, "Bandwidth, SAR, and efficiency of internal mobile phone antennas," *IEEE Trans. Antennas Propag.*, Vol. 46, No. 1, 71–86, 2004.
8. Kouveliotes, N. K., P. J. Papakanellos, E. D. Nanou, N. I. Sakka, V. S. G. Tsiafakis, and C. N. Capsalis, "Correlation between SAR, SWR and distance of a mobile terminal antenna in front of a human phantom: theoretical and experimental validation," *JEMWA*, Vol. 17, No. 11, 1561–1581, 2003.
9. Derat, B., J.-Ch. Bolomey, and C. Leray, "On the existence of a lower bound of SAR value for GSM mobile phone — a resonator-based analysis," *Proc. of JINA 2004 — Int. Symp. on Antennas*, 320–321, Nice, France, Nov. 8–10, 2004.
10. Chu, L. J., "Physical limitations of omnidirectional antennas," *J. App. Phys.*, Vol. 19, 1163–1175, 1948.
11. Collin, R. E. and S. Rotschild, "Evaluation of antenna Q," *IEEE Trans. Antennas Propag.*, Vol. 12, No. 1, 23–27, 1964.
12. Fante, R. L., "Quality factor of general ideal antennas," *IEEE Trans. Antennas Propag.*, Vol. 17, No. 2, 151–155, 1969.
13. Harrington, R. F., "Effect of antenna size on gain, bandwidth and efficiency," *J. Res. Nat. Bur. Stand.*, Vol. 64D, 1–12, 1960.
14. Hansen, R. C., "Fundamental limitations of antennas," *Proc. IEEE*, Vol. 69, 170–182, 1981.
15. McLean, J. S., "A re-examination of the fundamental limits on the radiation Q of electrically small antennas," *IEEE Trans. Antennas Propag.*, Vol. 44, 672–676, 1996.

16. Derat, B. and J.-Ch. Bolomey, "A new equivalent junction model for characterizing power absorption by lossy scatterers in reactive field regions," *Proc. of ANTEM 2005 — 11th Int. Symp. on Antenna Tech. and Applied Electromagnetics*, 344–345, Saint-Malo, France, June 15–17, 2005.
17. Derat, B. and J.-Ch. Bolomey, "Nouveau modèle de jonction équivalente pour l'analyse de l'absorption par un objet dissipatif en zone de champ proche réactif," *5th Scientific Days of CNFRS/URSI 2005*, <http://cnfrs.gettelecom.fr/actualites/Derat.pdf>, Paris, France, Feb. 24–25, 2005.
18. Derat, B. and J.-Ch. Bolomey, "Modal based comparison of dissipated power and SAR value for cylindrical and flat phantoms," *Proc. of ICONIC 2005 — 2nd Int. Conf. on Electromagnetic Near-Field Characterization and Imaging*, 335–340, Barcelona, Spain, June 8–10, 2005.
19. Lee, K. S. H and F.-C. Yang, "Trends and bounds in RF coupling to a wire inside a slotted cavity," *IEEE Trans. on EMC*, Vol. 34, No. 3, 154–160, 1992.
20. Harrington, R. F., *Time-Harmonic Electromagnetic Fields*, McGraw-Hill, New York, 1961.
21. Hansen, J. E., *Spherical Near-Field Antenna Measurements*, Peter Peregrinus, London, 1988.
22. Felbacq, D., G. Tayeb, and D. Maystre, "Scattering by a random set of parallel cylinders," *J. Opt. Soc. of Am. A*, Vol. 11, No. 9, 2526–2538, 1994.
23. Lancaster, P. and M. Tismenetski, *The Theory of Matrices*, 2nd Edition, Academic Press.
24. Böhm, M., J. Kremer, and A. K. Louis, "Efficient algorithm for computing optimal control of antennas in hyperthermia," *Surveys Math. Indust.*, Vol. 3, No. 4, 233–251, 1993.
25. IEC, "Procedure to measure to the Specific Absorption Rate (SAR) in the frequency range of 300 MHz to 3 GHz. Part I: Hand-held mobile wireless communication devices," IEC TC106/PT62209 (draft in progress).